Robotica: (2019) volume 37, pp. 1904–1921. © Cambridge University Press 2019
doi:10.1017/S0263574719000341

Tremor Estimation and Removal in Robot-Assisted Surgery Using Lie Groups and EKF

Rohit Rana†*, Prerna Gaur†, Vijyant Agarwal‡ and Harish Parthasarathy§

† *Instrumentation and Control Division, Netaji Subhas Institute of Technology, University of Delhi, New Delhi, India. E-mails: rohitrana982007@gmail.com, prernagaur@yahoo.com*
‡ *MPAE Division, Netaji Subhas Institute of Technology, University of Delhi, New Delhi, India. E-mail: vijayantonly@yahoo.com*
§ *Electronics and Communication Division, Netaji Subhas Institute of Technology, University of Delhi, New Delhi, India. E-mail: harisignal@yahoo.com*

(Accepted March 3, 2019. First published online: April 15, 2019)

SUMMARY
This paper aims at estimating the tremor torque using extended Kalman filter (EKF) applied to a two-link 3-DOF robot with nonlinear dynamics modelled using Lie-group and Lie-algebra theory. Later, it is generalised to d number of links with $(d + 1)$-DOF. The configuration of each link at any time is described by its rotation relative to the preceding link. Using this formulation, an elegant formula for the kinetic energy of the $(d + 1)$-DOF system is obtained as a quadratic form in the angular velocities with coefficients being highly nonlinear trigonometric functions of the angles. Properties of the Lie algebra generators and the Lie adjoint map are used to arrive at this expression. Further, the gravitational potential energy and the torque potential energy are expressed as nonlinear trigonometrical functions of the angles using properties of the SO(3) group. The input torque comprises a nonrandom intentional torque component and a highly nonlinear tremor torque component. The tremor torque is modelled as a stochastic differential equation (sde) satisfying Ornstein–Uhlenbeck (OU) process with diffusion and damping coefficients. Further, the tremor is treated as the disturbance. The Euler–Lagrange equations for the angles are derived. These form a system of sdes, and the EKF is used to get a more accurate disturbance estimate than that provided by the usual disturbance observer. The EKF is based on noisy angle measurements and yields as a bonus the angle and angular velocity estimates on a real-time basis. The parameters in the OU process model of the tremor torque, and parameters of the Fourier components of the intentional torque have also been estimated.

KEYWORDS: Tremor; EKF (extended Kalman filter); Lie group; Omni Bundle; Nonlinear phenomena; Surgical robots; OU process.

1. Introduction

Tremor is defined as involuntary, inconsistent and rhythmic movement of the body part. Generally, tremor can be categorized as rest tremor and action tremor. Furthermore, tremor is classified into two most common types, i.e. psychological tremor (PT) and essential tremor (ET).[1] Most of the tremor occurs in hands and makes life difficult, as it creates problems in eating, writing and other daily routines. It may become a social embarrassment issue for the people. Apart from the daily problems due to tremor, we face a significant threat in robot-assisted surgical operations as the significant

* Corresponding author. E-mail: rohitrana982007@gmail.com

https://doi.org/10.1017/S0263574719000341 Published online by Cambridge University Press

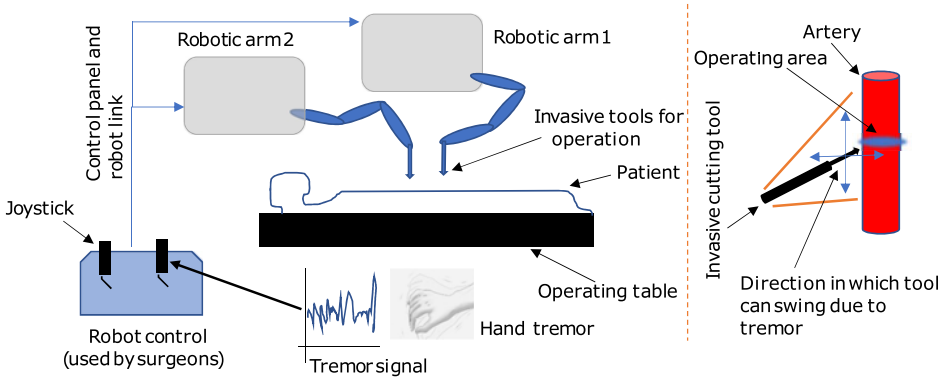


Fig. 1. Block diagram depicting robotic invasive surgery of human artery.

number of surgeons have the tremor in hands, for example, minimal invasive surgery (MIS) and retinal surgery.

Currently, the treatment of the tremor is done by using physiological and neurological drugs; in-depth brain simulations have also been used, but none of them guarantees a permanent solution.[2] Various robotic surgical tools were presented, developed and used to suppress the tremor. Most of the MIS are done using robots in master-slave mode as shown in Fig. 1. In this mode, the surgeon holds the joystick as a master and the slave robot end-effector is fitted with operating tools. As the master moves the joystick, the slave robot mimics the motion as of master. Another type of instruments used in surgeries is hand-held surgical devices such as Micron[3] and a sub-millimetre 3-DOF device,[4] in which the surgeon holds the single instrument for the surgery. In both the master-slave mode and the hand-held device mode, the tremor travels through the hands to the operating tools fixed on the robot. This may create a big problem during the surgical operation as the tools can swing away from the area of operation and cause damage to surrounding tissues. Therefore, it is necessary to remove the tremor from the salve end-effector.

Tremor is generally associated with the age factor and the physiological factor (example stress). Nearly, all good surgeons are on the higher side of the age and are in stress due to increased population burden. Therefore, they are more prone to tremor. If they operate with the tremor in invasive surgeries, the results could be highly unsuccessful. A robot-assisted surgery in the master-slave mode of the patient artery is depicted in Fig. 1. In the figure, it is clear that the tremor can cause the invasive tool to swing away from the area of operation. The swing may cause significant damage to surrounding tissues, resulting in an unsuccessful operation.

1.1. Literature review

In this section, we will consider the following three aspects of tremor torque. These aspects are the frequency of tremor torque, tremor torque suppressing methods and the dynamics modelling. Tremor acceleration data are measured by Trimmer et al. with a piezoelectric accelerometer sensor, and their studies reveal that tremor is a nonlinear stochastic process.[7] Furthermore, it is shown in that tremor can be considered as a diffusion process. The current methods to measure tremor are accelerometry, electromyography (EMG) and laser transducers. All these methods come with sensitivity and reliability problems. Portability and ease of use is another issue. Ramana Vijanmuri et al. presented a new glove device to extract features of hand tremors (note in 95% ET patents hands are affected[3]). In ref. [11], quantification is done by spectral analysis and time–frequency analysis. In the day-to-day activities, the intentional motion occurs in the frequency range 0–2 Hz, and tremor has a frequency range of 3–12 Hz. The fundamental and second harmonics tremor are concentrated over the range 4–6 Hz and 8–12 Hz. A 6-DOF microsurgical instrument[21] and Micron device[22] were developed to record and process the tremor data. Mainly, accelerometers were used to record the raw tremor data without the implementation of digital filters. Also no circuit tuning capability was present to remove the effect of noise on the raw sensor tremor data. There is substantial ambiguity in the tremor frequency, and data collection methods pushed us to verify the tremor frequencies.

https://doi.org/10.1017/S0263574719000341 Published online by Cambridge University Press

Previously, to suppress the tremor, energy socking soft material was used in robots. As a result, the intentional motion along with the tremor was suppressed. After soft-materials, mechanical loading becomes the alternative for tremor suppression. In mechanical loading, a semi-active or passive damper is developed by creating a resisting force using a brushless DC motor. Sanes et al. reported "suppressed the local tremor linearly" using a DC motor, through viscous damping in human wrists.[5] In Massachusetts Institute of Technology, the scientist has also tested control of action tremor by adding viscous and inertial load on limbs of the patients.[6] The frequency-locked loops were used to calculate stiffness and density of a particular tissue, through which the resisting force is calculated to suppress the tremor. The frequency-locked loop method purely depends on the frequency of tremor generated through a particular tissue, which differs from person to person. Therefore, the system needs to be tuned for different muscles according to the different persons, making it difficult to use.

Further, the linear filter algorithms were developed using weighted-frequency Fourier linear combiner (WFLC) filter[7] and notch filter[8] in exoskeleton termed as WOTAS system, in which the joint was moved in opposite direction to the tremor after estimating tremor through WFLC filter, cancelling the effect of tremor. The main disadvantage of linear filters is that these filters produce output with the constraint of linearity. Adaptive filter-based algorithms were developed to overcome the disadvantages of the linear filters. WFLC and band-limited multiple linear Fourier combiner (BMFLC) were proposed in refs. [9]–[11]. The filter techniques are very sensitive to noise, and even a small change in the frequency makes it difficult to track the tremor frequency. The tremor frequency changes with time and differs from person to person. Therefore, the filter techniques will not provide the desired results. In ref. [12], autoregression-based tremor methods were discussed. Multi-step prediction is also popular in tremor estimation and suppression. In refs. [13]–[15], multi-step prediction and time series forecasting have been applied with different versions of Kalman filters (EKF, UKF, etc.).

The next area of interest is the kinematics and dynamics modelling of the robot. At present, the modeling of dynamics and kinematics algorithms using classical robot theory is based on D–H parameters and solving differential equations. Another method to develop dynamics and kinematic modeling is by using Lie-group theory. Yang et al. [28] showed the significance of Lie-group theory in robot dynamics and kinematic modelling. The authors wish to formulate the problem using Lie-group theory because of its following advantages: first, the computational complexity will be reduced to a great extent. Second, the dynamics and kinematics of robot may be written in a more convenient and understandable form. Third, we can directly work on the variable of interest in Lie group and Lie algebra. Fourth, the error model for velocity profile of the robot is singularity free, as the kinematic parameters in robot models based on Lie group vary smoothly with the change in joint axis.[17]

In ref. [16], filter theory for Lie-group-valued stochastic processes is developed. The state takes X_t the values in a matrix Lie group G having Lie algebra g. Thus, its rate of change takes values in $Gg + Gg$ with the components in g describing noise and inputs. The measurement process is a function of the state in G and an iid measurement noise in $\mathbb{R}^p$ and takes values in an arbitrary space. The authors motivate this by an example of a rigid body with $G = SO(3)$. The authors discretize the model and transform it into a complete matrix multiplicative dynamical system, i.e. the state is an element of G, then they directly write down the group-theoretic Kalman filter for recursive state estimates. The advantage with this approach is that it is coordinate free and can be applied to Lie-group-based dynamical systems of any dimension. Our problem is however described in terms of the second-order differential equation for the rotation matrices $R(t) \leftarrow SO(3)$. Hence, to apply the results of ref. [16], it must be transformed to first-order differential equations on an enlarged group and then it could be used in problem formulation. Thus, we must enlarge our group $SO(3)$ to semidirect product $SO(3)$ and $so(3)$, where $g = so(3)$ is the Lie algebra of $SO(3)$.

The group transformation matrix of a multi-link robot regarding the translation, rotation and twist parameters is formulated in ref. [17]. The evaluation is based on the differential equation of the exponential map frequently used in Lie algebra theory. It provides a technique for identification of small parameter error vector like the change in the end effectors. The same method can be applied to our robotic system, by calculating the changes in specific points on the links regarding small changes in the Euler angles for each link. Further, if the Euler angles errors are modelled as random variables, then their covariance matrix can be estimated from repeated measurements in the errors in the positions of specific points on the links.

https://doi.org/10.1017/S0263574719000341 Published online by Cambridge University Press

In ref. [18], the theory of approximate group Lie symmetries for different equations has been developed. Given a differential equation, it may admit many point symmetries defined by Lie algebra generators and such symmetries enable us to find solutions of the differential equation easily. However, if this differential equation is perturbed by nonlinear terms tagged by perturbations parameters, then these symmetries may be broken. However, if we expand the solution to this perturbed equations as a Taylor series in the perturbation parameters, then the higher order perturbation terms satisfy linear equations driven by lower order perturbation terms. Such recursive equations may admit symmetries defined in terms of the independent variable and the different order perturbation terms of the dependent variable. Such symmetries are called approximate symmetries. These approximate symmetries enable us to find approximate solutions more efficiently. Approximate Lie generators symmetries can after be derived from the exact Lie generator symmetries of the unperturbed equation.

The Lie-group symmetries transformation method has been applied to the stochastic differential equations (sdes) in ref. [19]. The Brownian motion and Poisson process drive the sdes. Approximated transformation of the drift, diffusion and jump coefficient functions of the sde that guarantee invariance of the sde has been studied in detail by the author. The infinitesimal Lie transformation has been chosen so that the Brownian motion and Poisson statistics appearing in the sde remain invariant. Given any sde of the form $dX_t = f(t, X_t)dt + g(t, X_t)dB_t + h(t, X_t)dN_t$, where $f(t, X_t)dt$ is the diffusion term, $g(t, X_t)dB_t$ is the drift term and $h(t, X_t)dN_t$ is the jump term, we can make an infinitesimal transformation of time t, state variable X and also a random transformation of the Wiener process (B_t) and Poisson process (N_t), such that the statistics of the transformed Wiener process and Poisson process remain invariant (i.e. they satisfy the appropriate Ito's formula, and the sde satisfied by the transformed state $\bar{X}_t$ is also invariant). This enables us to obtain specific standard results like the random time change formula for Brownian motion. Oscillations can be controlled using this method as the following example shows: consider the sde $dX_t = V_t dt$ and $dV_t = -\omega^2 X_t dt + \epsilon f(X_t, V_t)dB_t$. This describes a harmonic oscillator with small random force $f(X_t, V_t)\frac{dB_t}{dt}$. To control it, we make an infinitesimal Lie transformation $\bar{X}_t = X_t + \epsilon\psi_X(t, X_t, V_t)$, $\bar{V}_t = V_t + \epsilon\psi_V(t, X_t, V_t)$ and $\bar{B}_t = B_t + \epsilon\psi_B(t, X_t, V_t)$ such that Ito's formula $d\bar{B}_t^2 = dt$ is preserved and $\bar{X}_t, \bar{V}_t$ satisfies similar equation up to $O(\epsilon)$, but with a different f (i.e. $\bar{f}(\bar{X}_t, \bar{V}_t)d\bar{B}_t$ replaces $f(x_t, V_t)dB_t$). Afterwards, a constant feedback force $\epsilon g_t(\bar{X}_t, \bar{V}_t)dt$ is provided so that after its incorporation (X_t, V_t) track a desired trajectory (X_t^d, V_t^d), better than what would be possible in the (X_t, V_t) domain (i.e. the transformed force $\bar{f}(\bar{X}_t, \bar{V}_t)$ is much smaller than $f(X_t, V_t)$ in magnitude resulting in smaller noise in the transformed process). Specifically, our transformed sde is obtained by using Ito's formula

$$d\bar{X}_t = dX_t + \epsilon\frac{\partial\psi_X}{\partial t}dt + \epsilon\frac{\partial\psi_X}{\partial X}dX_t + \epsilon\frac{\partial\psi_X}{\partial V}dV_t + \frac{1}{2}\frac{\partial^2\psi_X}{\partial V^2}\epsilon^2 f^2 dt + \frac{\partial\psi_X}{\partial V}\epsilon f dB_t$$

and likewise for V_t. The drift component of the control is $O(\epsilon)$ while the diffusion component is $O(\epsilon^2)$, so that drift will have more effect on average oscillation. If in addition there is a Poisson component, then our oscillation sde will have the form $dX_t = V_t dt$ and $dV_t = -\omega^2 X_t dt + \epsilon f(X_t, V_t)dB_t + \delta g(X_t, V_t)dN_t$. Ito's formula for $\bar{X}_t = X_t + \epsilon\psi_X(t, X_t, V_t)$ will now read

$$d\bar{X}_t = dX_t + \epsilon\frac{\partial\psi_X}{\partial t}dt + \epsilon\frac{\partial\psi_X}{\partial V}dV_t + \frac{1}{2}\epsilon^2\frac{\partial^2\psi_X}{\partial V^2}f^2 dt + \epsilon(\psi_X(t, X_t, V_t + \delta g(X_t, V_t)) - \psi(t, X_t, V_t))dN_t$$

Therefore, the jump noise effect on oscillation will be significant only if corresponding scale factor δ is large.

In ref. [23], it is not clear that the nonlinear oscillation of tremor is due to the nonlinear deterministic chaotic dynamics or from nonlinear stochastic dynamics. However, the paper was inclined towards the nonlinear stochastic second-order process. The reducibility approach solved the nonlinear sde, and the nonlinear dynamics of involuntary shaking of hand was provided in refs. [24, 27]. The linear and nonlinear characteristics of tremor were shown in ref. [25]. The chaos induced by random parameters in nonlinear systems and its solution using Melnikov technique is best explained in ref. [26], and thus enables us to get an insight about chaos in nonlinear systems.

https://doi.org/10.1017/S0263574719000341 Published online by Cambridge University Press

Now, it is evident that tremor is always considered as a noise or disturbance in the system, although the properties of tremor do not agree with this fact. Therefore, a model is needed for tremor torque in which it is not considered as noise. Instead, the tremor should be considered as a non-intentional torque because noise is neither intentional or non-intentional. In the MIS case, the noise always exists in any robotic system, but the tremor may or may not be present as it is a user input. The filtering methods discussed in the above literature review cannot be used, as all the filter methods considered tremor torque as noise. The advantages of Lie groups and Lie algebra are discussed, and there is a strong motivation that it should be used to derive system dynamics.

1.2. Problem statement

The goal of this paper is to estimate separately the intentional and non-intentional motion in the joystick operated surgical robot. Tremor is considered to be a non-intentional motion, in which the joystick motion is provided by the tremor affected human operator. The tremor-affected joystick motion is passed to the slave robot with surgical tools installed at the end effector. The non-intentional motion, i.e. the tremor should be removed from the robot. Only the intentional torque component should be passed to the robot. The model for intentional motion and tremor has to be derived in such a way that it should match the motion dynamics of human operator hands. The tremor sde is modelled as an Ornstein–Uhlenbeck (OU) process driven by the white Gaussian noise (WGN) with diffusion coefficients. The diffusion coefficients are driven by the mass moment of inertia matrix and a constant. The intentional motion is considered as a sum of sinusoids with different amplitudes, phases and frequencies. The convergence rate of the tremor model is also being considered, as the faster rate of convergence may provide the better results.

1.3. Overview of the paper

For the dynamics modelling of the robot, the Lie-group and Lie-algebra theory is used. The configuration of the robot used for the formulation purposes is the same as given in Fig. 4b. To obtain the Euler–Lagrange equations of motion the kinetic and potential energies are calculated. Later, the Euler–Lagrange equations of motion are generalized to a $(d+1)$-DOF robot, with d number of links. The hand tremor torque $\tau_k^T(t)$ is modelled as a disturbance satisfying OU process, which represents the nearly same amount of non-linear properties as present in the real hand tremor torque. The OU process is used to model the signal, which may have continuous to highly discontinuous states. It is further explained in Section 2.2.1. The tremor sde is driven by the white Gaussian noise (WGN) with the diffusion coefficients. The diffusion coefficients depend on the mass moment of inertia matrix and a constant.

For faster and better convergence of the tremor sde, the sde is further specialized with state-dependent damping coefficients to get the final tremor sde. The intentional motion torque $\tau_k^I(t, \underline{\alpha})$ is assumed to be the sum of sinusoids with different amplitudes, frequencies and phases. The Euler–Lagrange equation of motion is formulated with the sum of intentional motion torque and tremor torque. Afterwards, to get an estimate of the intentional motion and tremor, the extended Kalman filter (EKF) is formulated. The unknown state vectors for the EKF are defined as $\underline{X}(t) = \left[\underline{\theta}(t)\ \underline{\dot{\theta}}(t)\ \underline{\tau}^T(t)\ \underline{\alpha}\ \underline{C}\right]^\top$, where $\theta(t)$ and $\dot{\theta}(t)$ are the angular position and angular velocities, α is the intentional motion torque parameters (amplitude, frequencies and phase), and C is the constant. The EKF provides good estimates of the intentional motion torque and tremor torque. After estimation, the tremor torque is removed from the robot working with surgical tools at the patient's end. The highlights of this work are provided below:

1) the tremor torque is modelled as a local OU process driven by WGN with diffusion and damping coefficients depend on the system state for faster convergence. The tremor torque OU process is defined as $d\tau_k^T(t) = -\sum_{j=1}^{d+1} C_{kj}\psi_{kj}(\underline{\theta}, \underline{\dot{\theta}}, \phi, \dot{\phi})\tau_k^T(t) + \sum_j \sigma_{kj}^T W_{kj}^T(t)$, where C_{kj} is constant, $\psi_{kj}(\underline{\theta}, \underline{\dot{\theta}}, \phi, \dot{\phi})$ is the state dependent function, $\tau_k^T(t)$ is the tremor torque and $\sigma_{kj}^T W_{kj}^T(t)$ is the diffusion term (i.e. differential Brownian motion with small perturbation). The generalized OU process with state-dependent coefficients has the form $dX_t = V_t dt$, $dV_t = -\gamma(X_t, V_t)V_t dt + \sigma(X_t, V_t)dB_t$, where γ, σ are small perturbations, X_t, V_t are the position and velocity, and dB_t is the differential Brownian motion.

https://doi.org/10.1017/S0263574719000341 Published online by Cambridge University Press

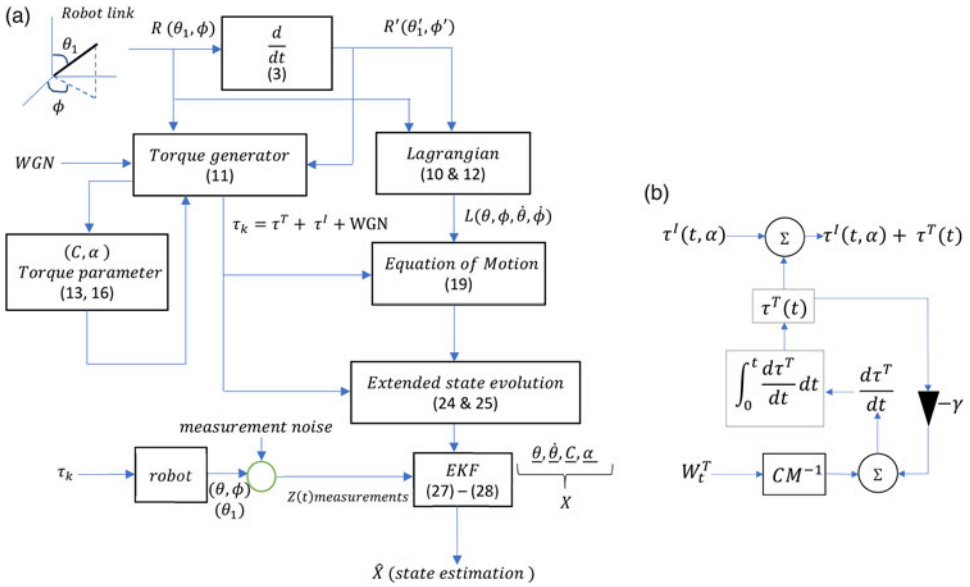


Fig. 2. (a) Block diagram of problem formulation section. (b) Inside view of *Torque generator* block shown in (a) (refer to Eq. 15).

2) Intentional motion torque is modelled as a sum of sinusoids with different amplitudes, frequencies and phases.
3) Robot dynamics is modelled using Lie groups and Lie algebra to reduce mathematical complexity.
4) The EKF is formulated to estimate the tremor torque as well as the intentional motion torque parameters.
5) The sensitivity to noise variance and parameters of uncertainty is also formulated and proved.
6) The final problem formulated algorithm is tested on the Omni bundle robot, which is generally used for training the human operator in the virtual surgical environment.

1.4. Organization of the paper

The problem formulation using Lie-group theory is provided in Section 2. Section 2.1 contains the dynamics modelling of d-link, $(d+1)$-DOF robot. The torque modelling is done in Section 2.2. Furthermore, Section 2.2 is divided into subsections 2.2.1 and 2.2.1, in which the tremor torque and intentional torque modelling is done. The EKF in implemented in Section 2.3. In Section 3, the stability and robustness is proved. The experimental simulations are implemented and explained in Section 4. Finally, concluding remarks are summarized in Section 5.

2. Problem Formulation

2.1. Dynamics modelling

The technique evolved in this paper is based on expressing the kinetic and potential energies of a $(d+1)$-DOF, with d number of links robotic system in terms of rotation matrices, which are parametrized by Euler angles. The first link has 2-DOF, and the rest of the links have 1-DOF, respectively. While writing down the Euler–Lagrange equations, we take into account tremor torque and intentional torque. The tremor torque is modelled along lines used in the literature review in Section 1, but with some additional features like the tremor torque observer error follows a version of local OU process. The EKF is then applied to the combined system that describes the Euler angles and disturbance observer evolution. Our approach to angle and tremor estimation can be viewed as a Lie-group, Lie-algebra approach since it uses properties or the Lie algebra of SO(3) to satisfy expressions in the derivation of the Lagrangian. The block diagram is shown as in Fig. 2, which shows the entire problem formulation in terms of blocks with their respective equations formulated in this section.

We first derive an expression for the kinetic energy of a two-link robot, where the first link has two DOF and the second link has one DOF. An arbitrary point r on the first link after time t is expressed as a rotation matrix acting on the initial position of the point. Let $R(t)$ is the rotation applied to the

https://doi.org/10.1017/S0263574719000341 Published online by Cambridge University Press

first link after time t. The rotation $R(t)$ can be expressed as $R_{\hat{y}'}(\theta_1(t))R_z(\phi(t))$, where $\hat{y}' = R_z(\phi)y$. Thus, $R(t) = R_z(\phi)R_y(\theta_1)$. Likewise, for the second link, the velocities of these points are obtained by differentiating these expressions with respect to time. The rotation applied to the second link relative to axes attached to a fixed point p on the first link is $S(t) = R_z(\phi)R_y(\theta_1 + \theta_2)$. If $\underline{p}$ is the point on the first link to which the base point of the second link is attached, then an arbitrary point $\underline{r}$ in the first link moves after time t to $\underline{r}(t) = \underline{\underline{R}}(t)\underline{r}$ and an arbitrary point $\underline{r}$ in the second link moves after time t to $\tilde{r}(t) = \underline{\underline{R}}(t)p + S(t)(\underline{r} - \underline{p})$. Here, r is the position vector of an arbitrary point within the robot at time $t = 0$, which after time t moves to the point $r(t)$ under the action of the rotation $R(t)$. The kinetic energies of the two links are calculated by integrating the magnitude squares of their velocity over the links. Then the kinetic energy of the first link can be written as

$$K_1 = \frac{1}{2}\rho \int_{B_1} ||r'(t)||^2 d^3r = \frac{1}{2}Tr(R'(t)JR'(t)^\top) \tag{1}$$

and the kinetic energy of the second link is expressed as

$$K_2 = \frac{1}{2}Tr(S'(t)J_2S'(t)^\top) + Tr(R'(t)J_{12}S'(t)^\top) + \frac{1}{2}Tr(R'(t)\tilde{J}_1R'(t)^\top) \tag{2}$$

In order to apply the theory of lie algebra, we need to express $R'(t)$ in the form $R(t).X(t)$, where $X(t)$ is a lie algebra element. The time derivative of each rotation matrix is expressed in terms of generators of SO(3) and the time derivatives of the rotation angle. Now from Eq. (2), using $R_z(\phi) = e^{\phi X_3}$ and $R_y(\theta_1) = e^{\theta_1 X_2}$ we get

$$R'(t) = R(t)(\dot{\theta}_1 X_2) + \dot{\phi}e^{\phi X_3}X_3e^{\theta_1 X_2} = R(t)z(t) \tag{3}$$

where $z(t) = \dot{\theta}_1 X_2 + \dot{\phi}(X_3 cos\theta_1 - X_1 sin\theta_1)$. Likewise $S'(t) = S(t)\tilde{z}(t)$, where $\tilde{z}(t) = (\dot{\theta}_1 + \dot{\theta}_2)X_2 + \dot{\phi}(X_3 cos(\theta_1 + \theta_2) - X_1 sin(\theta_1 + \theta_2))$. Thus, Eqs. (1) and (2) can be expressed as

$$K_1 = -\frac{1}{2}Tr(J_1z^2(t)) \text{ and } K_2 = -\frac{1}{2}(J_2\tilde{z}^2(t)) - Tr(S^\top(t)R(t)z(t)J_{12}\tilde{z}(t)) - \frac{1}{2}Tr(\tilde{J}_1z^2(t)) \tag{4}$$

Here, X_1, X_2, X_3 are the standard generators of the Lie algebra of SO(3) satisfying the commutation relations $[X_1, X_2] = X_3$, $[X_2, X_3] = X_1$, $[X_3, X_1] = X_2$. Writing $J_{10} = J_1 + \tilde{J}_1$, it follows from Eq. (4) that the total kinetic energy $K_1 + K_2$ of the two-link system can be expressed as

$$K = -\frac{1}{2}Tr(J_{10}z^2(t)) = -\frac{1}{2}Tr(J_2\tilde{z}^2(t) - Tr(S^T RzJ_{12}\tilde{z})) \tag{5}$$

This gives us an expression for the total kinetic energy of the link system as a quadratic function of time derivatives of the rotation matrices. Now consider the general case of a d-link system.The base point of the kth link is attached to a fixed point p_{k-1} on the $(k-1)$th link and after time t, a general point $\underline{r}$ in the kth link moves over to $R_1(t)p_1 + R_2(t)(p_2 - p_1) + \cdots + R_{k-1}(t)(p_{k-1} - p_{k-2}) + R_k(t)(\underline{r} - p_{k-1})$, $1 \le k \le d$, where $p_0 = 0$ and $R_k(t) = R_z(\phi(t))R_y(\theta_1 + \cdots + \theta_k(t)) = exp(\phi X_3)exp((\theta_1 + \cdots \theta_k)X_2)$. Thus, $R'_k(t)$ can be expressed as

$$R'_k(t) = R_k(t)(\dot{\phi}(t)cos(\theta_1 + \cdots \theta_k)X_3 - \dot{\phi}sin(\theta_1 + \cdots + \theta_k)X_1 + (\dot{\theta}_1 + \cdots + \dot{\theta}_k)X_2) \tag{6}$$

This equation can be expressed as $R'_k(t) = R_k(t)Z_k(t)$, where $z_k(t) = \Big(\sum_{j=1}^{k}\dot{\theta}_j\Big)X_2 - \dot{\phi}sin\Big(\sum_{j=1}^{k}\theta_j\Big)X_1 + \dot{\phi}cos\Big(\sum_{j=1}^{k}\theta_j\Big)X_3$. Therefore, the total kinetic energy of the kth link is

$$\tilde{K}_k = \frac{1}{2}\rho \int_{B_k} ||\sum_{j=1}^{k-1} R'_j(t)(\underline{p}_j - \underline{p}_{j-1}) + R'_k(t)(\underline{r} - p_{k-1})||^2 d^3r \tag{7}$$

$$\triangleq \frac{1}{2}Tr(R'_kJ_kR'_k(t))^T = -\frac{1}{2}Tr(J_kz_k^2(t)). \tag{8}$$

https://doi.org/10.1017/S0263574719000341 Published online by Cambridge University Press

We finally obtain the expression for the total kinetic energy of the link system, which is expressed as a quadratic function of the angular velocities with coefficients being trigonometric functions of the angles. The gravitational potential energy of the d-link robot is given by

$$V = M_1 g d_1 cos\theta_1 + M_2 g(p_1 cos\theta_1 + d_2 cos(\theta_1 + \theta_2)) + \cdots + M_k g(p_1 cos\theta_1 + p_2 cos(\theta_1 + \theta_2) + \cdots + p_{k-1} cos(\theta_1 + \cdots + \theta_{k-1}) + d_k cos(\theta_1 + \cdots + \theta_2)) + \cdots M_d g \left(\sum_{j=1}^{d-1} p_j cos(\theta_1 + \cdots + \theta_j) + d_d cos(\theta_1) + \cdots + \theta_d \right) \quad (9)$$

where d_k is the distance of the C.M of link k from its point of contact with the $(k-1)$th link. The Lagrangian in the absence of external input torque can be written as

$$L_0(\{\theta_k\}_1^d, \{\dot{\theta}_k\}_1^d, \phi, \dot{\phi}) = -\frac{1}{2} \sum_{k=1}^{d} T_r(J_k Z_k^2) - \sum_{1 \le j < k \le d} T_r(R_y \left(- \sum_{j+1}^{k} \theta_l \right) Z_j J_{jk} Z_k) - V. \quad (10)$$

2.2. *Torque modelling*

The torque on the kth link arising from the intentional torque and tremor torque in presence of the machine noise is expressed as

$$\tau_k(t) = \tau_k^I(t, \underline{\alpha}) + \tau_k^T(t) + \sigma_k \underline{W}_k(t), \quad (11)$$

where $\tau_k^I(t, \underline{\alpha})$ is the intentional torque component,$\tau_k^T(t)$ is the tremor component and $\sigma_k \underline{W}_k(t)$ is the machine noise component. We set $\phi = \theta_{d+1}$. The total contribution to the Lagrangian coming from the input torque is then

$$L_1(\{\dot{\theta}_k\}_{k=1}^d, \dot{\phi}, t) = \sum_{k=1}^{d} \tau_k(t)\dot{\theta}_k(t) + \tau_{d+1}(t)\dot{\phi}(t) = \sum_{k=1}^{d+1} \tau_k(t)\dot{\theta}_k(t). \quad (12)$$

2.2.1. *Tremor torque modelling.*

The tremor component of the torque has been modelled as a process to satisfy an OU sde driven by WGN. The sde diffusion coefficients depend on the mass moment of inertia matrix $M(\underline{\theta})$ and a constant matrix C. Following the general theory of the disturbance observers, the difference between the conventional disturbance observer[20] and the current one is the presence of damping coefficient and the assumption that the disturbance observer driver force is treated as WGN in our model. Thus, enables us to apply the EKF to this problem. The tremor torque $\tau_k^T(t)$ is treated as a disturbance d_t. The estimator dynamics can be expressed as $\hat{\dot{d}}_t = L(\underline{\theta}, \underline{\dot{\theta}})W_t$, where $L = CM(\theta)^{-1}$ and $W_t = (d_t - \hat{d}_t)$ (if $L(\underline{\theta}, \underline{\dot{\theta}}) > 0$, then estimator dynamics guarantees $(d_t - \hat{d}_t) \to 0$ as $t \to \infty$ provided that d_t as constant, $t \to \infty$). In the presence of damping, the standard disturbance observer (SDO) $\hat{\dot{d}}_t = L(\theta, \dot{\theta})W_t$,[20] modifies to $\hat{\dot{d}}_t = -\gamma \underline{\hat{d}}_t + LW_t$. Based on above SDO, the tremor torque modelled for $\tau_k^T(t)$ as a local OU process:

$$d\tau_k^T(t) = -\sum_{j=1}^{d+1} C_{kj} \psi_{kj}(\underline{\theta}, \underline{\dot{\theta}}, \phi, \dot{\phi}) \tau_k^T(t) + \sum_j \sigma_{kj}^T W_{kj}^T(t) \quad (13)$$

where $-\sum_j C_{kj} \psi_{kj}(\underline{\theta}, \underline{\dot{\theta}}, \phi, \dot{\phi})$ is the equivalent of $L = CM^{-1}$. Here, $d_t - \hat{d}_t$ is modelled as white noise and the diffusion coefficient is L. The stochastic model for the tremor torque based on 13 is the OU process satisfies

$$d\tau_k^T(t) = -\gamma_k \tau_k^T(t) + \sigma_k^T W_k^T(t) \quad (14)$$

https://doi.org/10.1017/S0263574719000341 Published online by Cambridge University Press

where $\gamma_k = \sum_{j=1}^{N} C_{kj}\psi_j(\theta, \dot{\theta}, \phi, \dot{\phi})$ and C_{kj} is constant, while the damping coefficients are state dependent. The C_{kj} constant depends on angular position and angular velocity. The disturbance observer equations become $L = CM^{-1}(\underline{\theta})$ and the tremor torque is further, expressed as

$$\frac{d\underline{\tau}^T(t)}{dt} = \underline{\underline{C}}M^{-1}(\underline{\theta}, \underline{\dot{\theta}})W_t^T - \gamma\tau^T(t) = \sum_{j,m=1}^{d+1} C_{kj}(M^{-1}(\underline{\theta}, \underline{\dot{\theta}})_{jm}W_m^T(t) - \gamma\tau_k^T(t) \tag{15}$$

This damped model is used for faster convergence of the tremor torque observer and is a special case of Eq. (13). If the damping coefficient is zero, then the driving white noise becomes simply the disturbance observer error. Here, now the state-dependent coefficients appear in the diffusion terms and the damping coefficients.

Equation (13) for the OU process can be written as $dX(t) = -\gamma X(t)dt + \sigma dB(t)$, where $X(t)$ is the state function and γ, σ are the parameters. If $\gamma, \sigma \to 0$, $\frac{\sigma}{\gamma} \to 1$, then $X(t) = \frac{\sigma}{\gamma}\frac{dB(t)}{dt}$. This shows that $X(t)$ is highly discontinuous and spiky. But when $\gamma \to 0$, $X(t) = B(t)$, making $X(t)$ as continuous and non-spiky. Therefore, the tremor is modelled as an OU process because it covers all states from continuous to discontinuous.

2.2.2. Intentional torque modelling.

Now a model for intentional torque is provided below. The model for intentional tremor is a sum of sinusoids with different frequencies and phases as unknown parameters to be estimated. Typically, we have p sources of power like p plug points generating signals of different frequencies. We can thus use these sources by appropriately linearly combining them to generate a control torque for tracking, or we may directly be using a linear combination of these sources which we wish to estimate via the EKF. Based on above, the following model for intentional torque is assumed:

$$\tau_i^I(t, \underline{\alpha}) = \sum_{j=1}^{p} A_{ij}\cos(\omega_j t + \phi_j),\ l \le i \le d+1 \tag{16}$$

where α is a set of parameters on which intentional torque can be adjusted. These include amplitudes, frequencies and phases of the sinusoid terms. The parameter vector $\underline{\alpha}$ is given by

$$\alpha = \left[Vec(\underline{\underline{A}}^\top)\ \underline{\omega}\ Vec(\underline{\underline{\phi}}^\top)\right]^\top \tag{17}$$

where $\underline{\underline{A}} = (A_{ij})_{1\le i\le d+1} \in \mathbb{R}^{(d+1)p}$, $\underline{\omega} = (\omega_j)_{j=1}^{p} \in \mathbb{R}^p$ and $\underline{\underline{\phi}} = (\phi_{ij})_{1\le i\le(d+1)}^{1\le j\le p} \in \mathbb{R}^{(d+1)p}$. The complete extended state equations, including the Euler–Lagrange equations, for the state $(\underline{\theta}, \underline{\dot{\theta}}, \underline{\phi}, \underline{\dot{\phi}})$ with intentional torques, tremor torque and noise terms can be formulated as

$$\frac{d}{dt}\left(\frac{\partial L_0}{\partial\dot{\theta}_k} - \frac{\partial L_0}{\partial\theta_k}\right) = \tau_K^I(t_1, \underline{\alpha}) + \tau_k^T(t) + \sigma_k W_k(t) \tag{18}$$

or equivalently

$$\sum_{j=1}^{d+1}\frac{\partial^2 L_0}{\partial\dot{\theta}_k\partial\dot{\theta}_j}\ddot{\theta}_j + \sum_{j=1}^{d+1}\frac{\partial^2 L_0}{\partial\dot{\theta}_k\partial\theta_j}\dot{\theta}j - \frac{\partial L_0}{\partial\theta_k} = \tau_k^I(t, \underline{\alpha}) + \tau_k^T(t) + \sigma_k W_k(t),\ 1 \le k \le d+1 \tag{19}$$

2.3. Extended Kalman filter

The extended state vector of the robot system $(\underline{\theta}(t), \underline{\dot{\theta}}(t))$, tremor torque, torque parameters $(\underline{\tau}^T(t), \underline{\alpha})$ and model parameters C vector is defined as $\underline{X}(t) = \left[\underline{\theta}(t)\ \underline{\dot{\theta}}(t)\ \underline{\tau}^T(t)\ \underline{\alpha}\ \underline{C}\right]^\top$. The equation of motion of the states and parameters can be cast in matrix notation as follows:

$$d\underline{\theta}(t) = \underline{\dot{\theta}}(t)dt \tag{20}$$

$$d\underline{\dot{\theta}}(t) = -M(\underline{\theta}, \underline{\dot{\theta}})^{-1}\underline{N}(\underline{\theta}, \underline{\dot{\theta}})dt + M(\underline{\theta}, \underline{\dot{\theta}})^{-1}(\underline{\tau}^I(t, \underline{\alpha}) + \underline{\tau}^T(t) + \sigma\underline{W}_\theta(t)) \tag{21}$$

https://doi.org/10.1017/S0263574719000341 Published online by Cambridge University Press

We now formulate the standard EKF-based observer for estimating the extended state on real-time basis. It should be noted that if we are given desired trajectory $X_d(t)$ to track, then we can input the consequent state feedback error to track the state trajectory keeping in mind that the robot state equations have derived from Lie-group–Lie-algebra-based representation of kinetic and potential energies with the Lie group being SO(3). The extended state equations for the parameters $\underline{\alpha}$, $\underline{\underline{C}}$ and the tremor torque τ_k^T can be formulated as

$$\frac{d\underline{\tau}^T}{dt}(t) = CM(\underline{\theta}, \underline{\dot{\theta}})^{-1}W^T(t) - \gamma\tau^T(t),\ \frac{dC}{dt} = \sigma_c W_c(t) \text{ and } \frac{d\alpha}{dt} = \sigma_\alpha W_\alpha(t) \tag{22}$$

The mass moment of inertia matrix $M(\underline{\theta}, \underline{\dot{\theta}})$ and the Coriolis and centrifugal matrix $N(\underline{\theta}, \underline{\dot{\theta}})$ can be expressed as

$$M(\underline{\theta}, \underline{\dot{\theta}}) = \left(\frac{\partial^2 L_0}{\partial\dot{\theta}\partial\dot{\theta}_j}\right)_{1\le i,j\le d+1} = \frac{\partial^2 L_0}{\partial\underline{\dot{\theta}}\partial\dot{\theta}^\top} \text{ and } N(\underline{\theta}, \underline{\dot{\theta}}) = \frac{\partial^2 L_0}{\partial\dot{\theta}\partial\theta^\top}\dot{\theta} - \frac{\partial L_0}{\partial\underline{\theta}} \tag{23}$$

Now, the system model is given by

$$dX(t) = F(t, X(t))dt + G(t, X(t))d\underline{B}(t) \tag{24}$$

where

$$F(t, X) = \begin{bmatrix} \underline{\dot{\theta}} \\ (-M^{-1}\underline{N} + M^{-1}(\tau^I(t,\alpha) + \tau^T)) \\ (-\gamma\tau^T) \\ \underline{0} \\ \underline{0} \end{bmatrix} \text{ and } G(t, X) = \begin{bmatrix} 0 & 0 & 0 & 0 \\ \sigma M^{-1} & 0 & 0 & 0 \\ 0 & CM^{-1} & 0 & 0 \\ 0 & 0 & \sigma_\alpha I & 0 \\ 0 & 0 & 0 & \sigma_c I \end{bmatrix} \tag{25}$$

$B(t) = \left[\underline{B}_\theta(t)\ \underline{B}^T(t)\ \underline{B}_C(t)\ \underline{B}_\alpha(t)\right]^\top \in \mathbb{R}^{(2(d+1)+(d+1)^2+p(2d+3))}$. Brownian motion $B(t)$ may take values from $(2(d+1)+(d+1)^2+p(2d+3))$. The coefficient of dt, i.e. $F(t, X, \theta_0)$ is called the drift coefficient and the coefficient of $dB(t)$, i.e. $G(t, X, \theta)$ is called the diffusion coefficient in the theory of Ito sdes. The measurement model is

$$dZ(t) = \underline{\theta}(t)dt + \sigma_v dV(t) \tag{26}$$

which means that we are taking only angular position measurements, and the EKF for X based on Z is derived below. The predicted state estimate and the predicted covariance matrix are expressed as

$$d\hat{X}(t) = F(t, \hat{X}(t))dt + \sigma^{-2}PH^T(dz - \hat{\theta}(t)dt) \tag{27}$$

$$\frac{dP(t)}{dt} = F'(t, \hat{X}(t)P(t) + P(t)F'^T(t, \hat{X(t)}) + (GG^T)(t, \hat{X}(t)) - PH^THP \tag{28}$$

where $H = [I_{d+1}|o]$ and $H^T = \left[\frac{I_{d+1}}{O}\right]$. The sde for $\hat{X}(t)$ shows that it is driven by the output feedback error $(dz - \hat{\theta}(t)dt)$. $F'(t, X) = \left[\frac{\partial F}{\partial\theta}\ \frac{\partial F}{\partial\dot{\theta}}\ \frac{\partial F}{\partial\tau^T}\ \frac{\partial F}{\partial\alpha}\ \frac{\partial F}{\partial C}\right]$ is the Jacobian matrix of the drift component of the sde satisfied by X, where explicitly the different blocks of this Jacobian are computed as follows:

$$\frac{\partial F}{\partial\tau^T} = \begin{bmatrix} 0 \\ M^{-1} \\ -\gamma I \\ 0 \end{bmatrix},\ \frac{\partial F}{\partial\alpha} = \begin{bmatrix} 0 \\ M^{-1}\frac{\partial\tau^I(t,\alpha)}{\partial\alpha} \\ 0 \\ 0 \\ 0 \end{bmatrix},\ \frac{\partial F}{\partial\underline{\theta}} = \begin{bmatrix} o \\ \frac{\partial}{\partial\theta}(M^{-1}N) - \frac{\partial M^{-1}}{\partial\theta}(I_{d+1}\otimes\tau^I + \tau^T) \\ \underline{0} \\ \underline{0} \\ \underline{0} \end{bmatrix},$$

$$\frac{\partial F}{\partial\underline{\dot{\theta}}} = \begin{bmatrix} I \\ M^{-1}\frac{\partial N}{\partial\dot{\theta}} \\ 0 \\ 0 \\ 0 \end{bmatrix} \text{ and } \frac{\partial F}{\partial C} = \begin{bmatrix} 0 \\ M^{-1}\frac{\partial\tau^T}{\partial C} \\ 0 \\ 0 \\ 0 \end{bmatrix} \tag{29}$$

https://doi.org/10.1017/S0263574719000341 Published online by Cambridge University Press

This brings to the end of tremor torque and intentional torque estimation and the EKF part.

3. Stability and Robustness

In this section, we present a new derivation that establishes conditions for stability robustness of a general EKF observer. By stability and robustness, we mean the sensitivity to noise variance and uncertainties in the parameters of observer error. The broad philosophy is as follows:

The state vector $\underline{X}(t)$ satisfies a sde whose drift and diffusion coefficients depend on some unknown parameters vector $\underline{\theta}_0$. The state observer $\hat{X}(t)$ satisfies a similar dynamics, but with no process noise (i.e. diffusion coefficient set is equal to zero). The drift coefficient is also the same and the unknown parameter replaced by a guessing parameter $\underline{\theta}$. The state observer is driven by the output estimation error as is done in the EKF. Assuming that our guess parameter is good, we suppose that $\delta_{\underline{\theta}} = \underline{\theta} - \underline{\theta}_0$ to be small and derive a sde for the observer error $\underline{X}(t) - \hat{\underline{X}}(t)$ in terms of $\delta_{\underline{\theta}}$ by the standard process of linearization and thereby obtain upper bounds on $\mathbb{E}||\underline{X}(t) - \hat{\underline{X}}(t)||^2$ in terms of $||\delta_{\underline{\theta}}||$. This is a precise result about the robustness of our observer w.r.t. parameter uncertainties. The state evolves according to the *sde* with actual parameters $\underline{\theta}_0$. The state is

$$d\underline{X}(t) = \underline{f}(t, \underline{X}(t), \underline{\theta}_0)dt + g(t, \underline{X}(t), \underline{\theta}_0)d\underline{B}(t) \tag{30}$$

The observer is constructed based on state space model but with a guess parameter $\underline{\theta}$. $\hat{L}_t$ is the observer gain, which in the case of EKF is chosen as $\hat{L}_t \equiv \sigma_v^2 P(t)^T\ h'(t, \hat{X}(t)^T)$, and $P(t)$ is the state error co-variance matrix. $P(t)$ is calculated using the Riccati equation (see Eq. 28). The observer is

$$d\hat{\underline{X}}(t) = \underline{f}(t, \hat{\underline{X}}(t), \underline{\theta})dt + \hat{L}_t(d\underline{z}_t - \underline{h}(t, \hat{\underline{X}}))dt \tag{31}$$

The approximate expression for the state estimation error obtained by linearizing the observer dynamics w.r.t. state and parameter around $\hat{X}(t)$ to θ_0 is

$$d\underline{z}_t = h(t, \underline{X}(t))dt + \sigma_v d\underline{V}(t) \tag{32}$$

Let $\underline{\theta} - \underline{\theta}_0 = \delta\underline{\theta}$ and $\underline{\theta}$ are the given parameters. The error between the state based on $\underline{\theta}_0$ and state based on $\underline{\theta}$ is given by

$$\underline{X}(t) - \hat{\underline{X}}(t) = \underline{e}(t) \tag{33}$$

Ito's formula gives stability for $d\underline{e}(t)$ from (34) followed by taking the expectation and using independence of the Browning increments $d\underline{B}(t)$ and $d\underline{V}(t)$ from $\{\hat{X}(s), s \leq t\}$ gives

$$d\underline{e}(t) = (\hat{F}_t - \hat{L}_t\hat{H}_t)\underline{e}_t - \underline{\underline{\hat{F}}}_{\theta}\delta\underline{\theta}dt + \underline{\underline{G}}_t d\underline{B}(t) - \sigma_v\hat{\underline{L}}_t d\underline{V}(t) \tag{34}$$

$$\mathbb{E}\{d(\underline{e}(t)\underline{e}^T(t))\} = \mathbb{E}[d\underline{e}(t)\underline{e}_t^T + \underline{e}(t)d\underline{e}(t)^T + d\underline{e}(t)d\underline{e}(t)^T] \tag{35}$$

$$\begin{aligned}\frac{d}{dt}\mathbb{E}(\underline{e}(t)\underline{e}(t)^T) = {} & \mathbb{E}\{(\hat{F}_t - \hat{L}_t\hat{H}_t)\underline{e}(t)\underline{e}(t)^T\} + \mathbb{E}\{\underline{e}(t)\underline{e}(t)^T(\hat{F}_t - \hat{L}_t\hat{H}_t)^T\} + \mathbb{E}(\hat{\underline{\underline{G}}}_t\hat{\underline{\underline{G}}}_t^T) \\ & + \sigma_v^2\mathbb{E}(\hat{L}_t\hat{L}_t^T) - \mathbb{E}(\hat{F}_\theta\delta\underline{\theta}\,\underline{e}(t)^T) - \mathbb{E}(\underline{e}(t)\delta\underline{\theta}^T\hat{F}_\theta^T)\end{aligned} \tag{36}$$

Let the maximum eigen value of $(\hat{F}_t - \hat{L}_t\hat{H}_t^T) + (\hat{F}_t - \hat{L}_t\hat{H}_t^T)^T$ be $-\lambda_0(\hat{X}_t) \equiv -\hat{\lambda}_0 < 0\ \forall\ \hat{X}_t$. Then,

$$\underline{e}(t)^T((\hat{F}_t - \hat{L}_t\hat{L}_t^T) + (\hat{F}_t - \hat{L}_t\hat{L}_t^T)^T)\underline{e}(t) \ \leq -\lambda_0(\hat{X}_t)\ ||\underline{e}(t)||^2 \tag{37}$$

where $||\ ||_s$ denotes the spectral norm. Thus, taking trace of (36), we get

$$\frac{d}{dt}\mathbb{E}||\underline{e}(t)||^2 \ \leq\ \lambda_{0\,min}\mathbb{E}||\underline{e}(t)||^2 + Tr\ \mathbb{E}\{(\hat{G}_t\hat{G}_t^T) + \sigma_v^2(\hat{L}_t\hat{L}_t^T)\} + 2||\hat{F}_\theta||_s\mathbb{E}||\underline{e}(t)||\ ||\delta_{\underline{\theta}}|| \tag{38}$$

where $\lambda_{0\,min} = min_{\hat{X}_t}\ \lambda_0(\hat{X}_t)$. Assume $max_t\ \ Tr\mathbb{E}\{\hat{G}_t\hat{G}_t^T + \sigma_v^2\hat{L}_t\hat{L}_t^T\} = \sigma^2 < \infty$ and $||\hat{F}_\theta||_s \equiv max_{\hat{X}_t}||\hat{F}_\theta(\hat{X}_t)||_s \equiv \alpha$. Let$\xi(t) = \mathbb{E}\{||\underline{e}(t)||^2\}$. Then since $\mathbb{E}\{||\underline{e}(t)||\} \leq \sqrt{\xi(t)}$, we get from (38)

https://doi.org/10.1017/S0263574719000341 Published online by Cambridge University Press

$$\frac{d\xi(t)}{dt} \leq -\lambda_{0min}\xi(t) + \sigma^2 + 2\alpha||\delta\underline{\theta}||\sqrt{\xi(t)} \tag{39}$$

Remark 1: We have assumed $\sigma^2(t) = Tr\mathbb{E}(G_t G_t^T + \sigma_v^2 L_t L_t^T) < \infty \; \forall \; t$ but it may grow unbounded with time. For example, if lnG_t or lnL_t have eigenvalues with positive real part. Therefore, imposing the constraint as $\sigma^2 = \sup_t \sigma^2(t) = \sup_t Tr\mathbb{E}(G_t G_t^T + \sigma_v^2 L_t L_t^T) < \infty$ is non-trivial, since it requires lnG_t and lnL_t to have eigenvalues with only negative real parts.
let $\sqrt{\xi}(t) = \eta(t)$. Then (39) reads $2\eta\eta' \leq -\lambda_{0min}\eta^2 + \sigma^2 + 2\alpha||\delta\underline{\theta}||\eta$ or $\eta' \leq -\frac{1}{2}\lambda_{0min}\eta + \frac{\sigma^2}{2\eta} + \alpha||\delta\underline{\theta}||$. Assume $\eta(t) \geq \eta_0 > 0 \; \forall t$. Then,

$$\eta'(t) \leq \frac{1}{2}\lambda_{0min}\eta + \frac{\sigma^2}{2\eta_0} + \alpha||\delta\underline{\theta}|| \tag{40}$$

Therefore,

$$\eta(t) \leq \exp(\frac{-\lambda_{0min}t}{2})\eta(0) + (\frac{\frac{\sigma^2}{2\eta_0} + \alpha||\delta\underline{\theta}||}{\frac{\lambda_{0min}}{L}})(1 - \exp(\frac{-\lambda_{0min}t}{2})) \tag{41}$$

and as $t \to \infty$, the RHS tends to $\frac{\sigma^2}{\eta_0\lambda_{0min}} + \frac{2\alpha}{\lambda_{0min}}||\delta\underline{\theta}||$. Thus, if the combined state α, measurement noise variance index σ^2 and the parametric uncertainty $||\delta\underline{\theta}||$ are small, then the state estimation error variance $\mathbb{E}(||e(t)||^2)$ is also small. This proves stability and robustness.
Remark 2: If $\eta(t) \geq \eta_0 \geq 0 \;\; \forall \;\; t$, i.e. $\eta(t)$ is bounded below by positive η_0, then Eq. (41) holds. On the other hand, if η_t is not bounded below by a positive number, then all $t \geq t_0$ (with arbitrary t_0) $\eta(t) \to 0$ as $t \to \infty$. So in either case $\eta(t)$ is upper bounded by Eq. (41) for all sufficiently large t.

4. Simulation and Experiments

4.1. Experimental setup

The experimental setup consists of a Omni™ Bundle 6-DOF robot connected with a computer via IEEE.1394 firewire port through USB to LAN adapter. QUARC® software and MATLAB™ software are installed on the computer. QUARC® software provides the connectivity between Omni Bundle and MATLAB. Three links of the Omni Bundle are actuated, and the other three are non-actuated as shown in Fig. 4a. Here, only three actuated joints are considered in a two-link configuration. The software simulation (off-line) and the hardware simulation (on-line) are implemented on MATLAB. The MATLAB simulated codes were directly converted into the Simulink functions. The same Simulink functions are implemented with Quarc Omni Bundle Simulink blocks to directly run on hardware robot through the external run option in Simulink.

The torque may consist tremor torque or intentional torque or both. The grounded Omni Bundle Simulink block in Fig. 3 shows that it is enabled for external torque input.

Furthermore, Fig. 3 shows the implementation of Fig. 2 and problem formulation as discussed in Sect.2. There are two manual switches which provide the capability to switch between external input torque and simulated output of tremor torque saved in the workspace as shown in Table I of this section. The EKF output $\hat{X}$ is saved in the workspace to analyze the output. In this experiment, only three actuated links are used, i.e. Omni Bundle is used in two-link configuration. The first link has 2-DOF and the second link has 1-DOF. The end effector of Omni Bundle indicates X, Y and Z coordinate positions. The link coordinate diagram is shown in Fig. 4b with respective lengths and angles.

4.2. Implementation

4.2.1. Software simulation. In this part, the position of switches is as per Table I, S. no. 4 (refer to Fig. 3). The WGN noise and the tremor torque parameters were fed in the OU-based process to generate tremor torque. Simultaneously the intentional torque is provided from workspace as a joint angle variable. The summation of both torques is fed in Lie-group-based Lagrangian equations of motion block. The measurement and state parameters are then fed into the EKF which estimates $\hat{\underline{X}}$. The estimated parameters are stored in the workspace for further evaluation

https://doi.org/10.1017/S0263574719000341 Published online by Cambridge University Press

Table I. Simulink switch working.

S. no.	Switch 1	Switch 2	State
1	*BOTTOM*	*BOTTOM*	*INVALID*
2	*TOP*	*BOTTOM*	*INVALID*
3	*BOTTOM*	*TOP*	$\tau_T^{*1} + \tau_I^{*2}$
4	*TOP*	*TOP*	$\tau_T^{*1} + \tau_I^{*1}$

| *1 – Simulated torque; *2 – Real torque |

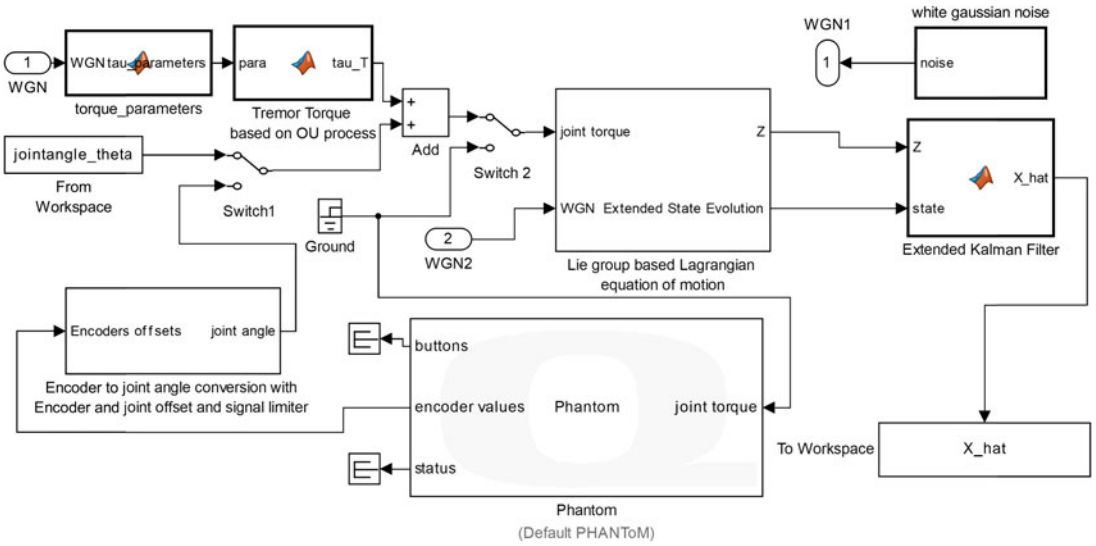


Fig. 3. MATLAB Simulink block diagram for real time simulation.

as discussed in the results section. To simulate the final group of equations provided in Eqs. (18)–(28), the following algorithms are used. For state model evolution algorithm 1 is provided, for measurement model algorithm 2 is used and finally for state estimation of EKF algorithm 3 is coded. The inertia matrix of Omni Bundle[29] is given as $M = \begin{bmatrix} m11 & m12 & m13 \\ m21 & m22 & m23 \\ m31 & m32 & m33 \end{bmatrix}$, where $m11 = k_1 1 + k_2 2cos(2\theta_2) + k_3 cos(2\theta_3) + k_4 cos(\theta_2) sin(\theta_3)$, $m12 = k5 sin\theta_2$, $m13 = 0$, $m21 = k5 sin\theta_2$, $m22 = k6$, $m23 = -0.5k4 sin\theta_2 - \theta_3$, $m31 = 0$, $m32 = -0.5k4 sin\theta_2 - \theta_3$, $m33 = k7.$, where $k_1 = 0.00179819707554751$, $k_2 = 0.000864793119787878$, $k_3 = 0.000486674040957256$, $k_4 = 0.00276612067958414$, $k_5 = 0.000308649491069651$, $k_6 = 0.00252639617221043$, $k_7 = 0.000652944405770658$, $k_8 = 0.164158326503058$, $k_9 = 0.0940502380783103$ and $k_{10} = 0.117294768011206$. The link lengths are $L_1 = 0.132$ m and $L_2 = 0.132$ m. The link masses are $M_1 = 0.035$kg and $M_2 = 0.1$ kg, respectively. The rest of parameters of Omni Bundle are given in ref. [30].

4.2.2. Hardware implementation. Hardware implementation is done in two parts to check the stability and robustness of the system. In first part, we assume that no noise is present in the system, only intentional torque and tremor torque are present. In second part, the system noise is also considered along with intentional torque and tremor torque. The noise is considered because in real hardware, noise can exist in the system and it may affect the robot stability. In system noise, two types of noises are considered, namely process noise and measurement noise. The first part is as follows: from Eq. (11) the total torque without system noise $\sigma_k W_k$ can be written as $\tau_k(t) = \tau_k^I(t, \alpha) + \tau_k^T(t)$. Similarly Eqs. (18) and 19 are modified. The algorithms 1, 2 and 3 are converted to the simulink functions for direct implementation in MATLAB simulink. The Omni Bundle robot can controlled through the simulink. The position of switches is as per Table I, S. no. 3 (refer to Fig. 3). The Omni Bundle simulink block is connected to ground signal, which enables it to receive external inputs. The

https://doi.org/10.1017/S0263574719000341 Published online by Cambridge University Press

Algorithm 1 State model algorithm

for t= 1:N **do**
  for k=1:d **do**
    $Sum = 0;$
    for j=1:d **do**
      $Sum = Sum + C(k,\ j) * \psi(\underline{\theta}(t), \underline{\theta}'(t));$
    $\gamma_k(t) = Sum;$
    $\gamma(t) = diag[\gamma_1(t), ...\gamma_d(t)];$
  $W_c(t) = randn(r);$
  $W_\alpha(t) = randn(\phi,\ 1)$ **No. of amplitudes, frequency & phases of sinusoidal intentional torques**
  $\underline{\underline{C}}(t+1) = \underline{\underline{C}}(t) + \sqrt{\delta} * \sigma_c W_c(t)$
  $\underline{\alpha}(t+1) = \alpha(t) + \sqrt{\delta} * \sigma_\alpha * \underline{W}_\alpha(t)$
  $\underline{\tau}^T[t+1] = C(t+1) * inv(M(\underline{\theta}(t), \underline{\theta}'(t)) * W_T(t) - \gamma(t) * \tau^T(t)$
  $X(t) = \begin{bmatrix} \underline{\theta}(t) \\ \underline{\dot{\theta}}(t) \\ \tau^T(t) \\ \underline{\underline{C}}(t) \\ \underline{\alpha}(t) \end{bmatrix}$
  $\underline{X}(t+1) = \underline{X}(t) + \delta * F(t, \underline{X}(t)) + G(t, \underline{X}(t))\sqrt{\delta} W(t)$

Algorithm 2 Measurement model algorithm

$Z(t) = 0;$
for t= 1:N **do**
  $V = randn(N+1,\ 1);$
  $Z(t+1) - Z(t) = \delta * \theta(t) + \sigma_v \sqrt{\delta} V(t+1);$
  for k=1:d **do**
    $Z(t+1) = Z(t) + \delta * \theta(t) + \sigma_v \sqrt{\delta} * V(t+1);$

Algorithm 3 EKF algorithm

for t= 1:N **do**
  $\hat{\underline{X}}(t+1) = \underline{X}(t) + \delta * \underline{F}(t, \hat{\underline{X}}(t)) + \underline{\underline{P}}(t) + \sigma_v^{-2} P(t) H^T (Z(t+1) - Z(t) - \hat{\theta}(t)\delta)$
  $\underline{\underline{P}}(t+1) = \delta * \underline{\underline{F}}'(t, \hat{\underline{X}})\underline{\underline{P}}(t) + \underline{\underline{P}}(t)\underline{\underline{F}}'(t, \hat{\underline{X}})^T + \underline{\underline{G}}(t, \hat{\underline{X}})\underline{\underline{G}}(t, \hat{\underline{X}})^T - \sigma_v^{-2}\underline{\underline{P}}(t) H^T H \underline{\underline{P}}(t)$
  where $\underline{\underline{H}} = \underline{\underline{h}}'(\hat{\underline{X}}(t))$ **and** $H^T H = \begin{bmatrix} \underline{\underline{I_d}} & \underline{\underline{0}} \\ \underline{\underline{0}} & \underline{\underline{0}} \end{bmatrix}$

input is provided to Omni Bundle robot in real time by the operator hand with substantial amount of tremor. The operator holds the third link (L_2) of the Omni Bundle, then the operator moves the end effector in the predefined trajectory (refer to Fig. 4a). The desired input trajectory is well explained in Fig. 5a. The torque signal received from the operator hand contains both intentional torque and tremor torque. Therefore, the output joint angles (ϕ, θ_k) contain both the tremor and intentional torques. These joint angular measurements are used to drive the EKF. The EKF is implemented using the group of Eqs. (20)–(29). The parameters in $\hat{\underline{X}}$ are then estimated.

In the second part, the total torque is considered as $\tau_k(t) = \tau_k^I(t, \alpha) + \tau_k^T(t) + \sigma_k W_k$. The magnitude of the noise is taken is 10^{-4} for both process noise and measurement noise. Rest of the procedure is followed as explained in the first part of the hardware implementation. The results for both the parts are discussed in Section 4.3.

4.3. Results

In Fig. 5a, the input signals to the Omni Bundle robot are plotted. In the highlighted part of the graph, the difference with tremor torque and without tremor torque can be seen. All the joint angles

https://doi.org/10.1017/S0263574719000341 Published online by Cambridge University Press

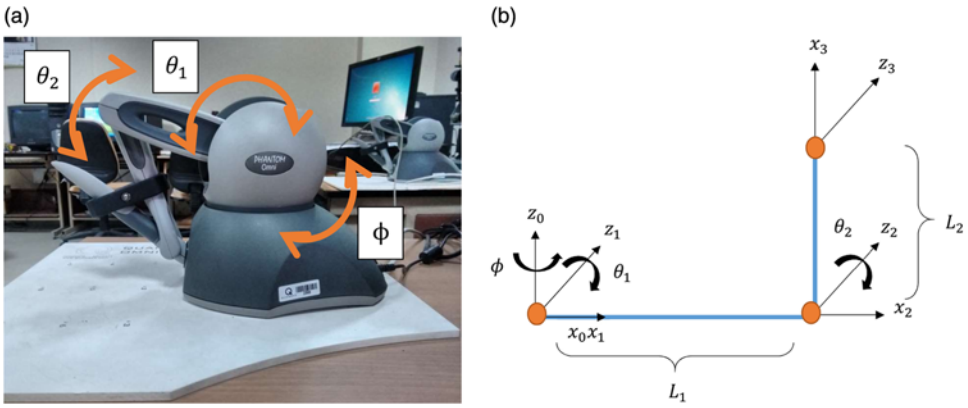


Fig. 4. (a) Sensable Omni Bundle^{TM} Robot. (b): Coordinate frames of Omni Bundle taken as two-link robot.

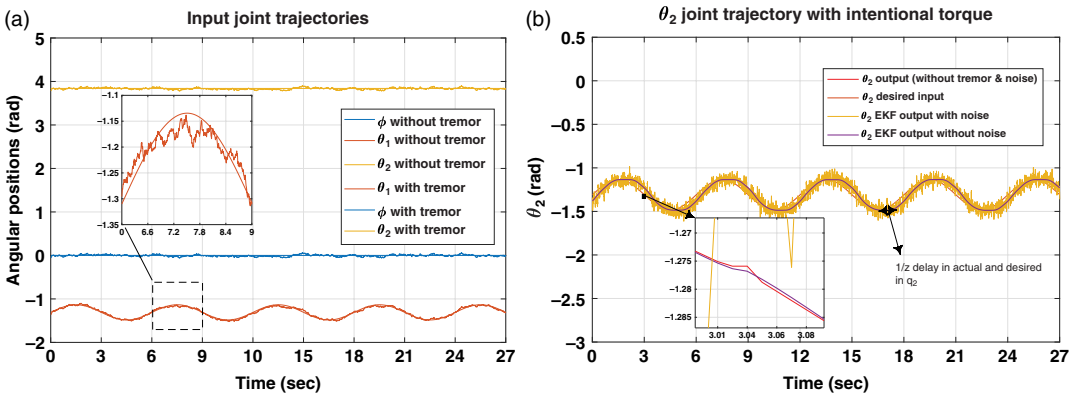


Fig. 5. (a) Graphical plot for input joint trajectories. (b) Response of joint θ_2 trajectory intentional torque.

ϕ, θ_1, θ_2 are shown in the graph. Although it may be noted that one angle ϕ (i.e link 1) is taken to be stagnant making it always zero. The θ_1 (i.e. link 2) is at certain angular position and the θ_2 (i.e. link 3) is moving up and down in straight line making a sine-wave pattern in the graph. In Fig. 5b, the θ_2 joint trajectory response with intentional and tremor torques as an input is shown with the actual trajectory, desired trajectory and EKF output with and without machine noise. Also, the θ_2 joint trajectory response with only intentional torque is given in Fig. 5b with EKF output with and without noise. From Figs. 5b and 6a, we can say that the tremor torque from the actual trajectory and the machine noise is substantially removed. Further, it can be concluded that the actual trajectory follows the desired trajectory. In Figs. 6b and 7a, the errors $e(t) = \hat{\theta}_2 - \theta_2$ is shown. Also, the proposed algorithm was also implemented and simulated in MATLAB and the output responses of implementation are given in Fig. 8a and 8b. Figure 8a and 8b shows that the proposed algorithm (previously tested on Omni Bundle) provides the similar results for both the cases (i.e. (1) only intentional torque and (2) intentional and tremor torque). The Matlab output figures also show that the EKF estimated joint angle $\hat{\theta}_2$ tracks the desired trajectory θ_2 with minimum error between actual and desired trajectories. The error plot for Fig. 8a and 8b is given in Fig. 7b. The error statistics for Fig. 7a are as follows: (1) without noise the statistics are [range = 0.2660, standard deviation = 0.0547 and mean value = 0.0017]. (2) With noise, the statistics are [range = 0.4474, standard deviation = 0.0720 and mean value = 0.0033]. The error statistics for Fig. 6b without noise are given as follows: (1) without tremor are [range = 0.1562, standard deviation = 0.0458 and mean value = $1.0909e^{-5}$]. (2) With tremor are [range = 0.4206, standard deviation = 0.0652 and mean value = 0.0016]. To the best knowledge of authors, the discussed hardware results with Omni Bundle are not reported in the literature.

https://doi.org/10.1017/S0263574719000341 Published online by Cambridge University Press

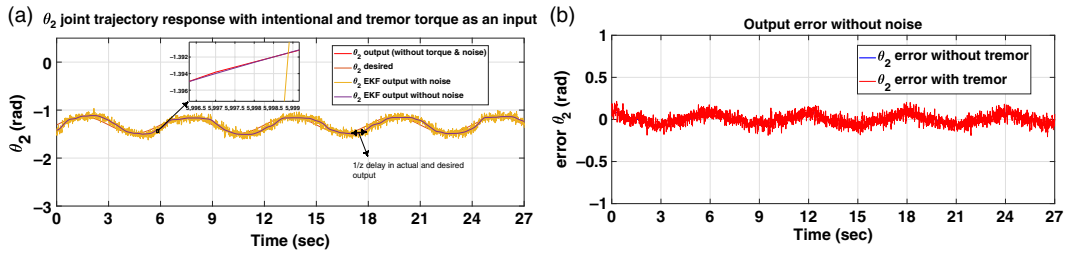


Fig. 6. (a) Response of joint θ_2 trajectory intentional torque and tremor torque. (b) θ_2 error plot with intentional torque and tremor torque.

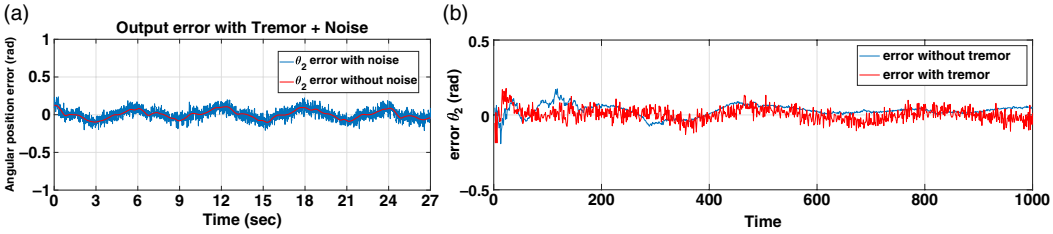


Fig. 7. (a) θ_2 error plot with intentional torque, tremor torque and noise. (b) Error plot for Fig. 8a and 8b.

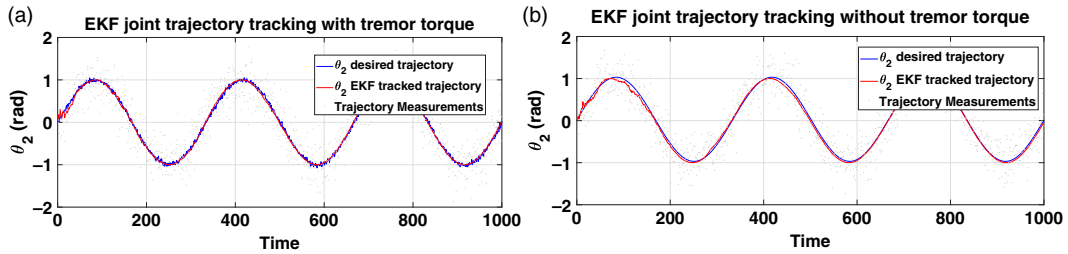


Fig. 8. (a) θ_2 input vs. output tracking plot with intentional torque and tremor torque. (b) θ_2 input vs. output tracking plot with intentional torque only.

5. Conclusion

In the literature, the tremor torque is considered as a noise along with the system noise leading to the less desirable results. For desirable results, the tremor torque should be treated separately from system noise along with the intentional torque. Further, for more desirable results the tremor torque model may be tuned using the tremor model coefficients. In this paper, only drift and diffusion terms are considered in tremor torque sde (based on OU process) without any Levy process (jump term). The generation of tremor torque from the tremor model can be controlled effectively using drift and diffusion coefficients as shown in Section 2.2. It is observed that the modelled tremor torque is significantly controlled by the drift term as compared to the diffusion term. The following are the novel features regarding estimating the nonlinear tremor torque in hand operated robot. The first feature is the expression for Euler–Lagrange with intentional torque, tremor torque in presence of the machine noise in terms of rotation matrices and their Lie algebra generators. The second novel feature is a model for tremor torque observer as an OU process, which in the limit of damping coefficients $\gamma \to 0$ becomes the conventional disturbance observer used in robotics with disturbance estimation error as WGN. The third novel feature is the application of the EKF to joint angular position and also the estimation of the parameters in the tremor torque model along with the parameters of the machine intentional torque. The fourth novel feature of this paper is a self-contained stability and robustness analysis of a state observer concerning noise variances and parameter uncertainties.

The proposed algorithm is tested by software and hardware experiments, and good agreement of hardware results with software simulated results is obtained. The following problem remains unsolved: The tremor torque sde analysis with drift, diffusion (including jump intensity) and jump terms (including jump amplitude).

https://doi.org/10.1017/S0263574719000341 Published online by Cambridge University Press

Conflict of Interest
The authors declare that they have no conflict of interest.

References

1. B. Taheri, D. Case and E. Richer, "Adaptive suppression of severe pathological tremor by torque estimation method," *IEEE/ASME Trans. Mechatron.* **20**(2), 717–727 (2015). doi:10.1109/TMECH.2014.2317948
2. D. Case, B. Taheri and E. Richer, "Design and characterization of a small-scale magnetorheological damper for tremor suppression," *IEEE/ASME Trans. Mechatron* **18**(1), 96–103 (2013). doi:10.1109/TMECH.2011.2151204
3. R. Vinjamuri, D. J. Crammond, D.Kondziolka, H-N. Lee and Z.-H. Mao, "Extraction of sources of tremor in hand movements of patients with movement disorders," *IEEE Trans. Inform. Technol. Biomed.* **13**(1), 49–56 (2009). doi:10.1109/TITB.2008.2006403
4. X. He, J. Handa, P. Gehlbach, R. Taylor and I. Iordachita, "A submillimetric 3-DOF force sensing instrument with integrated fiber Bragg grating for retinal microsurgery," *IEEE Trans. Biomed. Eng.* **61**(2), 522–534 (2014). doi:10.1109/TBME.2013.2283501
5. J. N. Sanes, P. A. LeWitt and K.-H. Mauritz, "Visual and mechanical control of postural and kinetic tremor in cerebellar system disorders," *J. Neurol. Neurosurg.Psychiatry* **51**, 934–943 (1988).
6. M. L. Aisen, A. Arnold, I. Baiges, S. Maxwell and M. Rosen, "The effect of mechanical damping loads on disabling action tremor," *Neurology* **43**, 1346–1350 (1993).
7. B. Taheri, D. Case and E. Richer, "Robust controller for tremor suppression at musculoskeletal level in human wrist," *IEEE Trans. Neural Syst. Rehabilit. Eng.* **22**(2), 379–388 (2014). doi:10.1109/TNSRE.2013.2295034
8. C. N. Riviere, S. G. Reich, and N. V. Thakor, "Adaptive Fourier modeling for quantification of tremor," *J. Neurosci. Methods* **74**(1), 77–87 (1997).
9. K. C. Veluvolu and W. T. Ang, "Estimation of physiological tremor from accelerometers for real-time applications," *Sensors* **11**, 3020–3036 (2011).
10. C. N. Riviere, W. T Ang and K. P. K, "Toward active tremor canceling in handheld microsurgical instruments," *IEEE Trans. Robot. Autom.* **19**(5), 793–800 (2003).
11. J. A. Gallego, E. Rocon, J. O. Roa, J. C. Moreno and J. L. Pons, "Real time estimation of pathological tremor parameters from gyroscope data," *Sensors* **10**, 2129–2149 (2010).
12. A. P. L Bo, P. Poignet, F. Widjaja, and W. T. Ang, "Online Pathological Tremor Characterization using Extended Kalman Filtering," *Proceeding on IEEE 30th Annual Internaltion Conference Eng. Med. Bio. Soc.*, Vancouver, Canada (2008) pp. 1753–1756.
13. S. G. Yuen, D. T. Kettler, P. M. Novotny, R. D. Plowes and R. D. Howe, "Robotic motion compensation for beating heart intracardiac surgery," *Int. J. Robot. Res.* **28**, 1355–1372 (2009).
14. S. Tatinati, K. C. Veluvolu and W. T. Ang, "Multistep prediction of physiological tremor based on machine learning for robotics assisted microsurgery," *IEEE Trans. Cybernetics* **45**(2), 328–339 (2015). doi:10.1109/TCYB.2014.2381495
15. K. Veluvolu, S. Tatinati, S.-M. Hong, W. Tech, "Multistep prediction of physiological tremor for surgical robotics applications," *IEEE Trans. Biomed. Eng.* **60**(11), 3074–3082 (2013). doi:10.1109/TBME.2013.2264546
16. A. Barrau and S. Bobnnabel, "Intrinsic filtering on Lie Groups with applications to attitude estimation," *IEEE Trans. Autom. Control* **60**(2), 436–449 (2015). doi:10.1109/TAC.2014.2342911
17. G. Chen, H. Wang and Z. Lin, "Determination of the identifiable parameters in robot calibration based on the POE formula," *IEEE Trans. Robotics* **30**(5), 1066–1077 (Oct. 2014). doi:10.1109/TRO.2014.2319560
18. R. Di Salvo, M. Gorgone and F. Oliveri, "A consistent approach to approximate Lie symmetries of differential equations", *Nonlinear Dyn.* **91**(1), 371–386 (2018). https://doi.org/10.1007/s11071-017-3875-5
19. A. M. Nass and E. Fredericks, "W-symmetries of jump-diffusion Itô stochastic differential equations," *Nonlinear Dyn.* **90**(4), 2869–2877 (2017). https://doi.org/10.1007/s11071-017- 3848-8
20. V. Agarwal and H. Parthasarathy, "Disturbance estimator as a state observer with extended Kalman filter for robotic manipulator", *Nonlinear Dyn.* **85**(4), 2809–2825 (2016).
21. S. Yang, R. A. MacLachlan and C. N. Riviere, "Manipulator design and operation of a six degree-of-freedom handheld tremor-canceling microsurgical instrument," *IEEE/ASME Trans. Mechatron.* **20**(2), 761–772 (2015). doi:10.1109/TMECH.2014.2320858
22. R. A. MacLachlan, B. C. Becker, J. C. Tabares, G. W. Podnar, L. A. Lobes and C. N. Riviere, "Micron: An actively stabilized handheld tool for microsurgery," *IEEE Trans. Robotics* **25**(1), 195–212 (2012). doi:10.1109/TRO.2011.2169634
23. J. Timmer, S. Hussler, M. Lauk and C.-H. Lcking, "Pathological tremors: deterministic chaos or nonlinear stochastic oscillators?" *Chaos* **10**(1), 278–288 (2000). doi:10.1063/1.166494
24. C. Zeng, Q. Yang and Y. Q. Chen, "Solving nonlinear stochastic differential equations with fractional Brownian motion using reducibility approach," *Nonlinear Dyn.* **67**(4), 2719–2726 (2012). https://doi.org/10.1007/s11071-011-0183-3
25. A. Yu Meigal, S. M. Rissanen, M. P. Tarvainen, S. D. Georgiadis, P. A. Karjalainen, O. Airaksinen and M. Kankaanp, "Linear and nonlinear tremor acceleration characteristics in patients with Parkinson's disease," *Physiol. Measurement* **33**(3), 395–412 (2012). doi:10.1088/0967-3334/33/3/395

https://doi.org/10.1017/S0263574719000341 Published online by Cambridge University Press

26. Y. H. Qin and J. C. Li, "Random parameters induce chaos in power systems," *Nonlinear Dyn.* **77**(4), 1609–1615 (2014). https://doi.org/10.1007/s11071-014-1403-4
27. O. E. Dick and A. D. Nozdrachev, "Nonlinear dynamics of involuntary shaking of the human hand under motor dysfunction," *Hum. Physiol.* **41**(2), 156–161 (2015). https://doi.org/10.1134/S0362119715010041
28. K. Yang, W. Yang, and C. Wang, "Inverse dynamic analysis and position error evaluation of the heavy-duty industrial robot with elastic joints: an efficient approach based on Lie group," *Nonlinear Dyn.* **93**(2), 487–504 (2018). https://doi.org/10.1007/s11071-018-4205-2
29. High-Level Control System for. Remote Controlled Surgical Robots. Haptic Guidance of Surgical Robot. Trondheim, June 2008. Master's thesis. NTNU.
30. R. Singla, H. Parthasarathy and V. Agarwal, "Classical robots perturbed by Lévy processes: analysis and Lévy disturbance rejection methods," *Nonlinear Dyn.* **89**(1), 553–575 (2017). https://doi.org/10.1007/s11071-017-3471-8

https://doi.org/10.1017/S0263574719000341 Published online by Cambridge University Press